Jestr

Journal of Engineering Science and Technology Review 16 (2) (2023) 37 - 48

Research Article

JOURNAL OF
Engineering Science and Technology Review

www.jestr.org

Determining the Global Response Characteristics of General Rotor/Stator Rubbing Systems with Hydrodynamic Forces

Huayi Cai[1], Shunzeng Wang[2,*] and Tao Li[3]

[1]*School of Electrical and Information Engineering, The University of Sydney, Sydney, NSW 2006, Australia*
[2]*School of Intelligent Manufacturing, Nanyang Institute of Technology, Nanyang 473006, China*
[3]*Department of Informatics, University of Zurich, Zurich 8050, Switzerland*

Received 19 December 2022; Accepted 2 April 2023

Abstract

Hydrodynamic forces caused by fluid-rotor interaction in fluid-rotor-stator systems can directly influence the occurrence of rubbing fault between the rotor and the stator, thereby affecting the stability of the rotating machinery. Considering the rotor-stator dynamics, the dry friction, and the flexibility on the contact surfaces as well as the fluid-rotor interaction, a 4D fluid-rotor-stator rubbing system was established to determine the global response characteristics exhibited in the general rotor/stator rubbing system with hydrodynamic forces. Aided by the features of orbits and full spectra, three types of rubbing responses were identified through experimental observation. The critical rotating speed of no-rub motion was analytically derived and confirmed by numerical simulation. Then, the global response characteristics on the parameter plane of the friction coefficient and rotating speed were numerically obtained. Results show that the critical rotating speed of no-rub motion decreases from 0.716 to 0.589 because of the hydrodynamic forces, and the coexistence of the partial rub with other responses is evident. From the influences of the system parameters, the decrease of the rotor mass has the same effect as increasing the rotor stiffness to mitigate rubbing responses. On the other hand, the increase of the rotor radius has the same effect as decreasing the clearance to increase the amplitudes of the rubbing responses. This study provides deeper insights into the highly detailed response characteristics of the general fluid-rotor-stator rubbing system.

Keywords: Rotor/stator rubbing, Hydrodynamic force, Critical rotating speed, Global response characteristics

1. Introduction

Rotor/stator systems are widely applied to basic rotating equipment, such as generator systems, motor systems, pump systems, gearbox systems, transmission systems, compressor systems, fan systems, turbocharger systems, steam turbines, and aircraft engines [1-3]. Besides, high-precision rotor/stator systems are also crucial to the highly effective and stable operation of micro-electro-mechanical systems, including magnetically levitated electric machines and compressors with nanometer size [4]. However, failure of the rotor/stator systems is inevitable because of manufacturing errors and/or complex operating conditions. The rotor/stator rubbing faults with impact and friction crops up frequently as a result of greater deformation than the clearance at the contact between the rotor and the stator. The risk of rotor/stator rubbing increases considerably as the clearances between the rotors and stators are decreased to enhance the efficiency and precision of the rotating machine to meet the demands of industrialization.

The rotor/stator rubbing is considered a secondary failure induced by the initial non-ideal factors and can introduce the most destructive responses [5]. During operation, large amplitudes of rotors and stators may be caused by the imbalance of rotors, misalignment of rotating shafts, deformation of stators, mutation of excitation and pyrocondensation of the clearance between the rotor and the stator, resulting in the rotor/stator rubbing [6]. During rubbing, the amplitude of the rotor can increase rapidly, not only during run-up and coast-down operations but also during the process with the rated speed, which can endanger the stable operation of rotating machinery. On the one hand, the circumferential and normal oscillation of the rotor/stator rubbing system is due to the friction at the contact between the rotor and the stator. An additional moment is attached to the circumferential whirling of the rotor because of the friction effect, which introduces the oscillation of the whirling speed and even the self-excited full annular backward whirl with large amplitude in the rotor/stator rubbing system. Besides, when the rotor is in continuous contact with the stator, an additional unstable support attached to the normal stiffness can trigger the nonlinear transient vibration of the critical speed and mode shape of the rotor. On the other hand, the complex and violent vibration is due to the impact and unstable excitation with the superposition of free vibration under certain conditions. Thus, the eccentricity of rotors and the local deformation of stators can be amplified to exacerbate the rotor/stator rubbing. In addition, the increase of the clearance resulting from the wear at the contact surfaces is also associated with a significantly increased likelihood of rubbing. Subject to continuous contact with the strong stress switching back and forth between the states of tension and compression in the rotor/stator rubbing system, the rotating equipment is prone to performance degradation and even destruction.

In practice, most rotor/stator systems are inseparable from the surrounding fluid, where fluid-structure interaction problems play a noteworthy role. The multidisciplinary

*E-mail address: httpwangji@163.com
ISSN: 1791-2377
doi:10.25103/jestr.162.06

nature of strong coupling and high nonlinearity remains a challenge in the comprehensive study of fluid-structural interaction. In the fluid-rotor-stator rubbing system, the interaction between the stator and the rotor in the surrounding fluid extracting specific features necessitates a thorough understanding of the fundamental physics that successively involve fluid-shaft coupling, mathematical model formulation, and numerical discretization [7]. The most appropriate numerical discretization is affected by the continuous model formulation of the fluid-rotor-stator rubbing system in the particular case in hand [8]. During whirling, the shape of the flow subdomain must change to accommodate the movements and deflections of the rotor and the stator in the fluid-rotor-stator rubbing system. Given the more complex conditions of the fluid-structural interaction, the differential equations of the fluid-rotor-stator rubbing system must satisfy the boundary conditions involved in the fluid and rotor domains. For most problems of the fluid-structure interaction, because analytical solutions of the governing equations are infeasible and laboratory equipment have limitations, conducting reliable numerical simulations helps to understand the rotor/stator rubbing fault involved in the fluid-rotor-stator system with hydrodynamic forces.

Based on the preceding analysis, this study explores a complex and difficult problem in the general fluid-rotor-stator system for the multiple degree-of-freedoms (DOF) and strong nonlinearity as well as the instantaneous switching from the impact to the continuous contact. From a practical point of view, it is significant for theoretical research and practical applications of rotating machinery on the complex dynamic responses and the corresponding parameter evolutions in the fluid-rotor-stator rubbing system. To this effect, in the four-DOF mathematical model of the general fluid-rotor-stator rubbing system involving the hydrodynamic force, both the dynamics of the rotor and the stator as well as the friction effect is established. Combined with the results of theoretical analysis and numerical simulation, the global response characteristics of the general fluid-rotor-stator rubbing system can be determined with the influences of the system parameters. The study provides a more comprehensive and deeper insight into the detailed response characteristics in the general rotor/stator rubbing systems with hydrodynamic forces.

2. State of the art

The complex phenomena of the rotor/stator rubbing induced by the imbalance of the rotor and/or the hydrodynamic force, specifically its mechanism and dynamic characteristics, have attracted scholarly attention related to mitigating the risk of rubbing fault. By analyzing the friction effect of rotating machinery in detail, Dimarogonas [9] first proposed that the friction characteristics and dynamic forces at the contact surfaces between the rotor and the stator are the main risk factors for the rotor/stator rubbing. Subsequently, based on the elastic model of the rotor/stator rubbing system, a series of studies on the physical phenomena and experimental results have been conducted [10-12]. Due to the nature of multiple DOF and strong nonlinearity in the rotor/stator rubbing system, a variety of contact responses have been captured, such as synchronous full annular rub, quasi-periodic whirl, and even the chaotic motion. Besides, studying the jump phenomenon and bifurcation in the rotor/stator rubbing system is also deemed intractable. According to the relative deflection of the rotor and the stator at the contact surfaces, the rubbing responses can be categorized into three typically continuous contact motions: no rub motion, partial rub with intermittent contact and synchronous full annular rub. Through experimental and numerical studies, knowledge on the inducing mechanism and existence boundaries of the rubbing responses has been obtained, and the influences of system parameters have also been explored. The numerical simulation is suitable for the analysis of the complex rubbing responses for the strong nonlinearity in the rotor/stator rubbing system. Li [13] introduced the evolutionary probability vectors into a generalized cell mapping for the global rubbing responses of the rotor/stator rubbing system with random variables. From the point of view of nonlinear normal mode, Wang [14] has deeply and comprehensively studied the stick-slip oscillation caused by friction effect in the rotor/stator rubbing system through theoretical analysis and numerical simulation. In addition, the effect of the cross-coupling stiffness of the rotor [15], the bending-torsional coupling [16] and the rough deformation of the contact surfaces [17] in the rotor/stator rubbing system have also been fully discussed. In view of this, the dynamic analysis of a rotor/stator rubbing system with midspan and overhung discs [18] and of a multi-modal rotor/stator rubbing system [19] was also conducted, and the 3D finite model of the rotor/stator system [20] has been a focus of research. To comprehensively reveal the nonlinear responses and parameter influences of the rotor/stator rubbing system, the dynamic analysis is generally on the simplified model based on the Jeffcott rotor system where many realistic factors, such as the fluid-structural interaction, are omitted

At present, only a few studies on the vibration of rotating machinery within the surrounding fluid have been furnished [21,22]. Kadyrov [23] had studied the oscillation of a rigid cylinder in a cylindrical duct filled with an incompressible viscous fluid subjected to different parameters through mathematical analysis. Taking into account the nonlinear stiffness of the bearings and the vibrations of fluid and the foundation in a rotor-fluid-foundation system, Kydyrbekour [24] established the generalized dynamic model and derived the optimization parameters for reducing the stress at the contact surfaces, the forced vibration amplitude and the instable range. Tchomeni and Alugongo [25] investigated the complex fluid-rotor interaction induced by the elastic vibration of the unbalanced rotor under rubbing and cracking in the viscous fluid as parametric excitation. A new algorithm and wavelet denoising technique were applied to extract the features of the cracked rotor system in viscous fluid medium. It was found that the hostile frequencies that could initiate and expand the crack and the lateral deflection shapes of the rotor were mainly triggered by the viscous fluid forces. Based on the different fluid properties including the inviscid and highly viscous fluid, as well as three different geometric structures, Gomes and Lienhart [26] analyzed the self-excited modal responses of the flexible structures in the uniform flow with different Reynolds numbers. The dynamic characteristics of the structures in the sequence of modes were confirmed as the function of the structure characteristic in the flow. Recently, the rubbing fault with the interaction between the oil-film forces and the rotor/stator system has been known to be one of the most common destructive malfunctions of rotating machinery [27]. Thus, distinguishing the mechanism of the rubbing responses in the fluid-rotor-stator system is an important task. Considering the hydrodynamic forces and friction in

the clearance between the rotor and the ring, Banakh and Nikiforov [28] studied the features of the interaction between the rotor and the floating sealing ring. Most recently, many experiments on the dynamic stability of the fluid-rotor-stator system have been conducted to elicit the empirical results. Through experimental analysis, Zhu [29] shed light on the dynamic characteristics of the overhung rigid rotor system partially filled with fluid. The influence of viscous fluid-fill ratio on the whirling frequency of the rotor, the unstable region and the rotor unbalance were all elucidated. From the experimental results of the submerged and confined disc with rotating fluid on the lower surface, Hengstler [30] observed that the fluid was rotating with respect to the standing disc. By the aid of the disc test apparatus in which the rotating disc was excited by a piezoelectric patch and submerged into the heavy fluid both in rotating and stationary frames, Presas [31] concluded that the rotating disc submerged into the heavy fluid exhibited different behaviors from those of the rotor/stator system with dry friction, for instance, the transmission from whirling to stationary phase. However, a reasonable explanation of the mechanism of the various behaviors is lacking. In general, current studies mostly address the influences of the fluid properties on the responses of the rotor/stator system. In particular, the global response characteristics of the general fluid-rotor-stator rubbing system are still in their infancy when the fluid-rotor interaction occurs.

Therefore, considering the dynamics of the rotor and the stator, the dry friction and flexibility on the contact surfaces, as well as the fluid-rotor interaction, on the general fluid-rotor-stator rubbing system is established to characterize the global response characteristics as the variation of the system parameters and initial conditions in the study.

The remainder of this study is organized as follows. In Section 3, the mathematical model of the general fluid-rotor-stator rubbing system considering hydrodynamic forces and both the dynamics of the rotor and the stator is introduced, and the inherent features of the orbits and full spectrum of the rubbing response are discussed. In Section 4, with the aid of the critical rotating speed that rubbing occurs in the general fluid-rotor-stator rubbing system, the existence conditions of the rubbing responses are obtained though theoretical analysis and numerical calculations. In Section 5, the influences of mass ratio and stiffness ratio and rotor radius on the relative deflection between the rotor and stator are studied in the general fluid-rotor-stator rubbing system. Finally, conclusions are drawn in Section 6.

3. Methodology

The coordinate system of a fluid-rotor-stator rubbing model with the rotor submerged in the inviscid fluid is defined as shown in Fig. 1, where O denotes the inertia coordinate center of the flexible shaft, O_r is the geometric center of the rotor, O_s is the geometric center of the stator, ω is the rotating speed of the rotor, ω_w is the whirling speed of the rotor with respect to the stator, e is the eccentricity vector of attached unbalance mass m_r, $r_r = \sqrt{x_r^2 + y_r^2}$ is the deflection of the rotor, $r_s = \sqrt{x_s^2 + y_s^2}$ is the deflection of the stator, $|r_r - r_s|$ is the relative deflection between the rotor and the stator, r_d is the rotor radius, and r_0 is the clearance between the rotor and the stator. The modified Jeffcott rotor model consists of a weightless shaft which is supported in ideal bearings with the effective transverse stiffness k_r. An annular stator of mass m_s is concentric with the disk and elastically supported by a symmetrical set of springs with isotropic radial stiffness k_s. According to the deformation at the contact surfaces between the rotor and the stator, a symmetrical set of fictive springs with isotropic radial stiffness k_b is supposed to be laid in the inner ring of the stator as the surrogate contact stiffness.

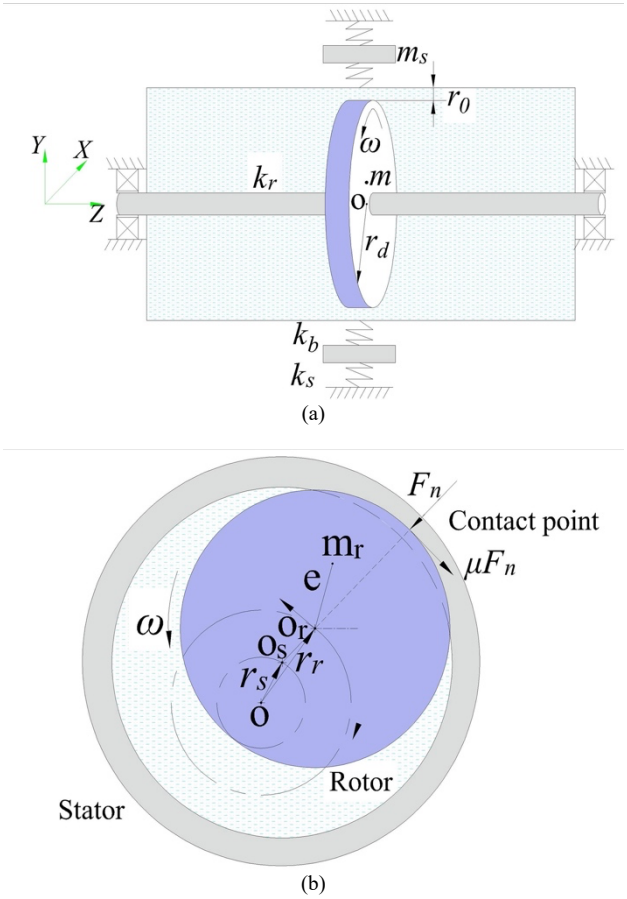

Fig. 1. (a) Illustration of fluid-rotor-stator model interacting with a point-mass stator across a clearance. (b) Rotor/stator interaction motion. The inviscid fluid is colored in cyan

The free-body diagram of the general fluid-rotor-stator rubbing system in contact is shown in Fig. 1(b), where the instantaneous location of the disk on the shaft in contact with the stator at contact point is also shown. Considering the hard surface of the disk and the stator, without damping, the different snubbing forces stemming from either the Coulomb friction element or unilateral springs acts on the rotor and the stator are drawn. The pointing direction of the friction force with the friction coefficient μ depends on the tangential direction of the relative velocity between the rotating speed ω and the whirling speed ω_w. In the present analysis, an excitation simulating the rubbing forces is included in the model and generated a piecewise smooth system equation with the neglect of the gravity and the coupled interaction between the springs k_s and k_b. The DOF of the lumped system on the disc accounts only for a rigid-body rotation and two orthogonal lateral defections.

Rubbing occurs if $|r_r - r_s| \geq r_0$, the relative velocity v_{rel} at the contact point may be less than the wheel peripheral speed $r_d\omega$ when the rotor whirls backward with a negative

ω_w. Furthermore, the relative velocity v_{rel} can be negative, implying the change of its direction, because of the backward procession with a negative frequency and the relative deflection of sufficient magnitude. Thus, the discontinuous smoothness is generated in the general fluid-rotor-stator rubbing system. The normal force F_n and tangential force F_μ during rubbing can be respectively expressed as:

$$\begin{cases} F_n = k_b(|\, r_r - r_s \,| - r_0) \\ F_\mu = \text{sign}(v_{rel})\mu F_n \\ v_{rel} = r_d\omega + |\, r_r - r_s \,|\, \omega_w \end{cases} \tag{1}$$

where the function $\text{sign}(v_{rel})$ implies a sign change of the relative velocity and is multivalued at $v_{rel} = 0$ with sign(0) = [-1, 1].

Based on the origin O with respect to the disc body coordinate system (X, Y), the snubbing forces F_n and F_μ respectively acting on the rotor and the stator can be rewritten in the X and Y directions as:

$$\begin{cases} F_{xr} = -F_{xs} \\ \quad = k_b(1 - \dfrac{r_0}{|\, r_r - r_s \,|})[(x_r - x_s) - \text{sign}(v_{rel})\mu(y_r - y_s)] \\ F_{yr} = -F_{ys} \\ \quad = k_b(1 - \dfrac{r_0}{|\, r_r - r_s \,|})[(y_r - y_s) + \text{sign}(v_{rel})\mu(x_r - x_s)] \end{cases} \tag{2}$$

where subscripts *r* and *s* are for the rotor and stator components, respectively.

In the general fluid-rotor-stator rubbing system, the inviscid fluid motion generated from rotor motion provokes the liquid hydrodynamic forces acting on the rotor, which can be obtained by integrating the pressure distribution in a rectangular tank under bending vibration. Provided that the incompressible and initially irrotational fluid motion is at low Reynolds number induced by small-amplitude oscillation in the first mode of the rotor/stator system, the derivation of the hydrodynamic forces acting around the rotating shaft under sinusoidal lateral excitation is established in this study as discussed in [15], neglecting the hydrostatic pressure and the participation in the shaft motion.

Based on the 2D analysis of fluid motion in a rectangular container of depth *h* and width *l* as shown in Fig. 1, the hydrodynamic forces acting along the X and Y axis can be determined from the pressure equation as follows [9,10].

$$\begin{cases} F_{xfluid} = m_f x_{r0}\omega_f{}^2 \cos\omega_f t \cdot \\ \qquad [1 + \dfrac{2l\omega_f{}^2}{(\zeta_f{}^2 - 1)(\omega_{fn}{}^2 - \omega_f{}^2)} \cdot \dfrac{\tanh(\zeta_f h / l)}{\zeta_f h}] \\ F_{yfluid} = -m_f y_{r0}\omega_f{}^2 \sin\omega_f t \cdot \\ \qquad [1 + \dfrac{2l\omega_f{}^2}{(\zeta_f{}^2 - 1)(\omega_{fn}{}^2 - \omega_f{}^2)} \cdot \dfrac{\tanh(\zeta_f h / l)}{\zeta_f h}] \end{cases} \tag{3}$$

where x_{r0}, y_{r0}, and ω_f respectively represent the excitation amplitude and frequency; m_f is the total mass of the fluid; and ζ_f is the damping factor of the fluid in the first mode with the natural frequency ω_{fn} of the liquid free surface.

From the assumption of the first mode with $x_r = x_{r0}\cos\omega_f t$ and $y_r = y_{r0}\sin\omega_f t$, the hydrodynamic forces induced by the rotor motion can be rewritten as:

$$\begin{cases} F_{xfluid} = m_{ff}\ddot{x}_r \\ F_{yfluid} = -m_{ff}\ddot{y}_r \\ m_{ff} = m_f[1 + \dfrac{2l\omega_f{}^2}{(\zeta_f{}^2 - 1)(\omega_{fn}{}^2 - \omega_f{}^2)} \cdot \dfrac{\tanh(\zeta_f h / l)}{\zeta_f h}] \end{cases} \tag{4}$$

Eq. (4) includes nonlinear inertia terms represented by the total mass m_f of the fluid. From the first asymmetric mode of the rotor, $\zeta_f = 0.01441$ [10].

By introducing the fluid hydrodynamic forces into the fluid-rotor-stator rubbing system and performing some suitable manipulations, we can formulate the force relation of the lateral vibration through the following differential equations:

$$\begin{cases} (m_r - m_{ff})\ddot{x}_r + c_r\dot{x}_r + k_r x_r + \Theta k_b(1 - \dfrac{r_0}{|\, r_r - r_s \,|})[(x_r - x_s) - \text{sign}(v_{rel})\mu(y_r - y_s)] = m_r e\omega^2\cos\omega t \\ (m_r + m_{ff})\ddot{y}_r + c_r\dot{y}_r + k_r y_r + \Theta k_b(1 - \dfrac{r_0}{|\, r_r - r_s \,|})[(y_r - y_s) + \text{sign}(v_{rel})\mu(x_r - x_s)] = m_r e\omega^2\sin\omega t \\ m_s\ddot{x}_s + c_s\dot{x}_s + k_s x_s - \Theta k_b(1 - \dfrac{r_0}{|\, r_r - r_s \,|})[(x_r - x_s) - \text{sign}(v_{rel})\mu(y_r - y_s)] = 0 \\ m_s\ddot{y}_s + c_s\dot{y}_s + k_s y_s - \Theta k_b(1 - \dfrac{r_0}{|\, r_r - r_s \,|})[(y_r - y_s) + \text{sign}(v_{rel})\mu(x_r - x_s)] = 0 \\ v_{rel} = r_d\omega + |\, r_r - r_s \,|\, \omega_w \end{cases} \tag{5}$$

where c_r and c_s are respectively the effective damping constants of the rotor and the stator. Θ is Heaviside function with $\Theta = 0$ when $|\, r_r - r_s \,| < r_0$ and $\Theta = 1$ when $|\, r_r - r_s \,| \geq r_0$.

The fluid-rotor-stator rubbing model represented by Eq. (5) is subject to the friction effect, contact deformation, dynamics of the rotor and stator, as well as fluid effect of the hydrodynamic forces. Moreover, the proposed model can be degenerated to the general rotor/stator rubbing system by omitting the effect of the fluid hydrodynamic forces stemming from the contact surface of the container wall and around the bottom [12], i.e., $m_{ff} = 0$. Furthermore, this model can be degenerated to the following three simpler

fluid-rotor-stator systems by considering the effect of the radial forces stemming from the support and/or the contact surface of the stator, i) a fluid-rotor-stator rubbing for a pinned stiff stator by fixing $k_s=\infty$ and $k_c=\infty$; ii) a fluid-rotor-stator rubbing for a pinned flexible stator by fixing $k_s=\infty$; and iii) a fluid-rotor-stator rubbing for a stiff stator based on flexible support by fixing $k_c=\infty$.

Then, Eq. (5) is reformulated into the non-dimensional form as:

$$\begin{cases}(1-M_{ff})X_r''+2\zeta_r X_r'+X_r+\Theta\beta_{cr}(1-\dfrac{R_0}{|R_r-R_s|})[(X_r-X_s)-\text{sign}(V_{rel})\mu(Y_r-Y_s)]=\Omega^2\cos\Omega\tau\\ (1+M_{ff})Y_r''+2\zeta_r Y_r'+Y_r+\Theta\beta_{cr}(1-\dfrac{R_0}{|R_r-R_s|})[(Y_r-Y_s)+\text{sign}(V_{rel})\mu(X_r-X_s)]=\Omega^2\sin\Omega\tau\\ M_{sr}X_s''+2\zeta_s\sqrt{M_{sr}\beta_{sr}}X_s'+\beta_{sr}X_s-\Theta\beta_{cr}(1-\dfrac{R_0}{|R_r-R_s|})[(X_r-X_s)-\text{sign}(V_{rel})\mu(X_r-X_s)]=0\\ M_{sr}Y_s''+2\zeta_s\sqrt{M_{sr}\beta_{sr}}Y_s'+\beta_{sr}Y_s-\Theta\beta_{cr}(1-\dfrac{R_0}{|R_r-R_s|})[(Y_r-Y_s)+\text{sign}(V_{rel})\mu(X_r-X_s)]=0\\ V_{rel}=R_d\Omega+|R_r-R_s|\Omega_w\end{cases} \tag{6}$$

where $M_{sr}=m_s/m_r$, $M_{ff}=m_{ff}/m_r$, $X_r=x_r/e$, $Y_r=y_r/e$, $X_s=x_s/e$, $Y_s=y_s/e$, $R_r=r_r/e$, $R_s=r_s/e$, $R_0=r_0/e$, $R_d=r_d/e$, $\beta_{cr}=k_b/k_r$, $\beta_{sr}=k_s/k_r$, $2\zeta_r=c_r/\sqrt{m_r k_r}$, $2\zeta_s=c_s/\sqrt{m_s k_s}$, $\omega_0=\sqrt{k_r/m_r}$, $\Omega=\omega/\omega_0$, $\Omega_w=\omega_w/\omega_0$, $\tau=\omega_0 t$, and prime represents the derivative with respect to the non-dimensional time τ in which ω_0 is the natural frequency of the rotor system with zero clearance.

According to Eq. (6), the relative velocity V_{rel} at the contact point can be either positive or negative. As a result, the friction force can switch its direction correspondingly according to the term of V_{rel}. So, $V_{rel}=0$ is also termed as the discontinuous boundary or switching manifold, which divides the phase space of the fluid-rotor-stator rubbing system into two smooth regions. Considering the friction effect and the contact stiffness, we find that a positive or negative sign of the relative velocity V_{rel} corresponds to a backward or forward direction of the friction force exhibiting a positive or negative damping. Thus, numerous vibration phenomena of the fluid-rotor-stator rubbing system might be induced, including backward whirl, which is a full or partial annular backward whirl at a negative super-synchronous whirl frequency Ω_w. Physically, the relative deflection $|R_r-R_s|$ fluctuates asymmetrically in the sense of the softening value of the inertia force in X-axis and the hardening value of that in Y-axis because of the hydrodynamic forces.

4 Result Analysis and Discussion

4.1 Dynamics of the fluid-rotor-stator model

In the following, the response scenario of the general fluid-rotor-stator rubbing system governed by Eq. (6) is simulated numerically with varying of rotating speed Ω. The orbits of the rotor, the stator, and the relative deflection between them, as well as the full spectrum can all be obtained by the classical fourth-order Runge-Kutta algorithm. In simulations, the responses are numerically calculated by integrating Eq. (6) with the specific initial conditions on the rotor and stator at the fixed rotating speed Ω. The time step of 10^{-3} is adopted to integrate Eq. (6) until the steady-state solutions are found. Then, the solution information of 60 (non-dimensional time) is recorded with the positions and velocities of both the rotor and the stator.

In all the examples presented below, the other system parameters are chosen according to the parameters of a test rig, whose existence condition and whirl frequency have been examined in [12,21]. The following system parameters are always fixed as:

$$\begin{aligned}&\zeta_r=0.02,\ \zeta_s=0.01,\ M_{sr}=2.0526,\ \beta_{cr}=20,\\ &\beta_{sr}=15.319,\ R_0=1.05,\ R_d=2.66R_0\end{aligned} \tag{7}$$

with $\mu\in[0,0.4]$ and $\Omega\in[0,3]$.

When the friction coefficient is taken as $\mu=0.4$ and the coefficient of the fluid hydrodynamic force is also set as $M_{ff}=0.2$, the global bifurcation diagram of Eq. (6) with the variation of Ω is captured through the forward sweep with the rotating velocity increasing from 0 to 3 and the backward sweep with the rotating velocity decreasing from 3 to 0, as shown in Fig. 2.

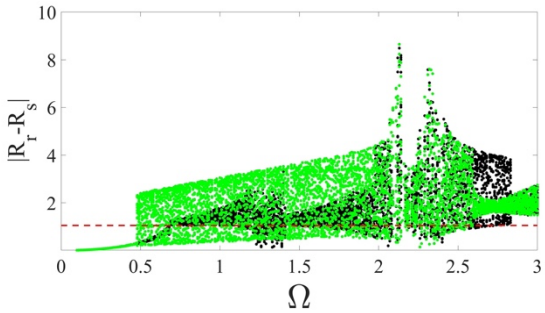

Fig. 2. Global bifurcation diagram of general fluid-rotor-stator rubbing system with variation of Ω. The black points indicate forward process, the green points represent reverse process, and the red dashed line is R_0

As shown in Fig. 2, two different response branches exist, indicating the increase and decrease of the rotating speed of the rotor in the range of $\Omega\in[0,3]$. When the relative deflection between the rotor and the stator is greater than the clearance, i.e., $|R_r-R_s|\geq R_0$, the rotor/stator rubbing occurs. The black points for forward process in the diagram show that the scenario of rotor responses with the increase of rotating speed is illustrated as no-rub motion

with $|R_r - R_s| < R_0$ → a partial rub with $|R_r - R_s| \le R_0$ and $|R_r - R_s| \ge R_0$ → a heavy rub with $|R_r - R_s| > R_0$ in the general fluid-rotor-stator rubbing system, which corresponds well with the theoretical and experimental results of the rotor/stator rubbing system with dry friction reported in [5,15]. The present study shows that the rotor/stator rubbing can be triggered because of only the mass imbalance if the rotating speed reaches a certain value in the general fluid-rotor-stator rubbing system. It is also observed from the green points for the backward process that the rotor/stator rubbing, once generated by the imbalance, could be maintained in a wide range of rotating speeds, especially until a very low rotating speed that is much lower than the critical rotating speed of the case with the increase of the rotating speed. This rubbing feature is also found in the rotor/stator rubbing system with dry friction [5,15].

With the aid of the orbits of the rotor, the stator and relative deflection between them, as well as the full spectrum, the response characteristics of the general fluid-rotor-stator rubbing system with the zero initial condition, through specific numerical examples, are illustrated. Fig. 3 exemplifies the orbits and the full spectra of the representative rotor/stator responses in the development process into the heavy rub. The orbits are formed of interlaced circular loops in shape, which can be employed to detect the presence of rubbing deflection. In the general fluid-rotor-stator rubbing system with inviscid fluid, the weak rubbing can partly distort ellipses of orbits as shown in Fig. 3.

Fig. 3(a) shows the response of no-rub motion of the general fluid-rotor-stator rubbing system at $\Omega = 0.4$, which can occur during $\Omega \in [0,\ 0.68]$ as illustrated for the case in Fig. 2. The deflection R_r of the rotor is represented by the black orbit with the clearance R_0 between the rotor and the stator by the dashed red line. The orbits show that only the deflection R_r of the rotor is discerned with $R_r < R_0$ because of the unbalanced mass. In the full spectrum of the rotor, the positive frequency component $\Omega_w = 0.4$ corresponding to the rotating speed is dominant, which coincides with our knowledge. As the rotor sustains a negative constant phase angle in this response, namely, a phase lag of the rotor center to the imbalance, the imbalance serves as an excitation that tends to drive the rotor to whirl forward.

Fig. 3(b) shows the response of the partial rub of the general fluid-rotor-stator rubbing system at $\Omega = 1$, which can occur during $\Omega \in [0.68, 2.74]$ as illustrated for the case in Fig. 2. The deflection R_s of the stator is represented by the magenta orbit with the relative deflection $|R_r - R_s|$ by the blue. Due to the asymmetrical fluctuation in the X and Y axes, the rotor and the stator orbit in ellipses. The deflection R_r of the rotor is greater than R_0, i.e., $R_r > R_0$, while the deflection R_s of the stator and the relative deflection $|R_r - R_s|$ are both partly greater than R_0. In the full spectrum of the rotor, a negative whirl frequency, i.e., $\Omega_w = -2$, appears and indicates that the backward whirl of the rotor is opposite its forward rotation. The whirling is twice the rotating speed, i.e., $\Omega_w = 2\Omega$, which is also discerned through the experimental studies in [22]. According to the negative whirl frequency with larger magnitude than that of the harmonic excitation at $\Omega = 1$, the energy of the backward whirl dominantly comes from the nonlinear mode motion rather than the forced excitation.

Fig. 3(c) shows the response of the heavy rub of the general fluid-rotor-stator rubbing system at $\Omega = 2.7$, which can occur during $\Omega \in [2.74,3]$ as illustrated for the case in Fig. 2. The relative deflection $|R_r - R_s|$ is much greater than R_0, i.e., $|R_r - R_s| >> R_0$, with R_r and R_s partly greater than R_0 showing a full annular rub. In the full spectrum of the rotor, a negative whirl frequency, i.e., $\Omega_w = -4.1$, appears and indicates that the backward whirl of the rotor is opposite its forward rotation. According to the almost similar magnitudes of the negative whirl frequency and the positive excitation frequency $\Omega = 2.7$, the contribution of the harmonic excitation is as important as that of the nonlinear modal motion in the continuous rub.

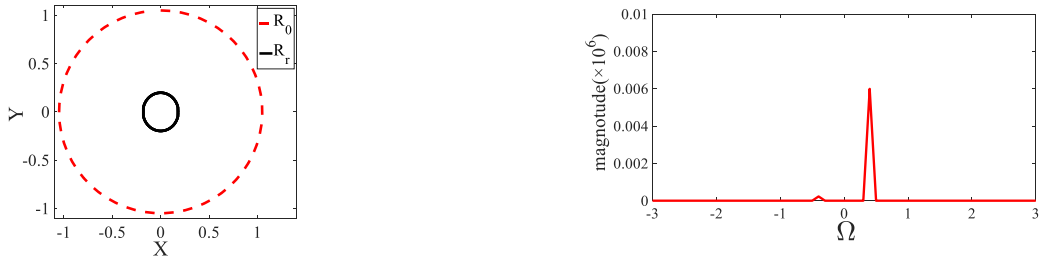

(a) $\Omega = 0.4$

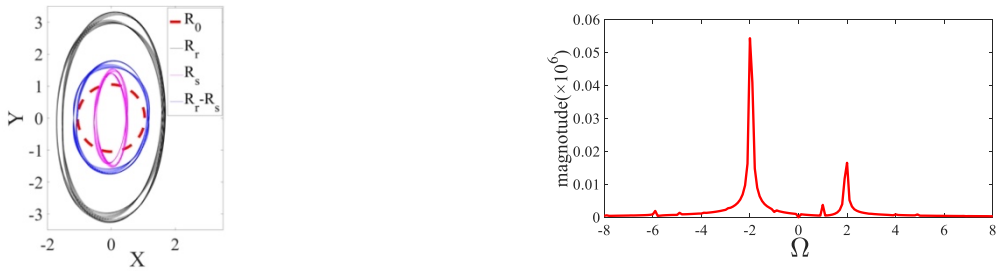

(b) $\Omega = 1$

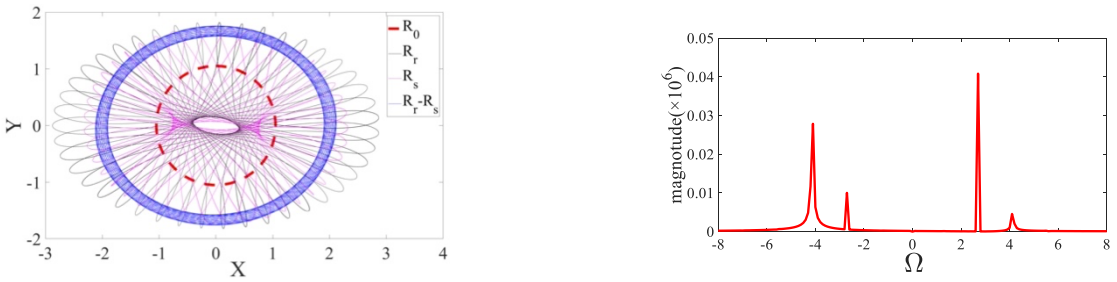

(c) $\Omega = 2.7$

Fig. 3. Rotor/stator orbits and full spectrum at different rotating speeds with system parameters as depicted in Eq. (7). (a) No rub, (b) partial rub, and (c) heavy rub, where it is supposed that the friction coefficient $\mu = 0.4$ and the coefficient of the fluid hydrodynamic force $M_{ff} = 0.2$

According to Figs. 2 and 3, the only synchronous no-rub motion occurs in the low rotating speed range, i.e., $\Omega < 0.48$, and the coexistence of the rubbing responses is found when $\Omega \geq 0.48$. In this case, as illustrated in Fig. 2, the coexistence of no-rub motion and partial rub occurs when $0.48 < \Omega < 0.69$, while one can find the region where the partial rub coexists with the heavy rub when $2.59 < \Omega \leq 2.74$.

In addition, irregular dynamic behaviors remain during the partial rubbing in the general fluid-rotor-stator rubbing system as shown in Fig. 4. The orbits of the rotor, stator, and relative deflection between them, exhibits irregularly quasi-periodic curves that have been confirmed to occur near the critical speed of the general fluid-rotor-stator rubbing system [22].

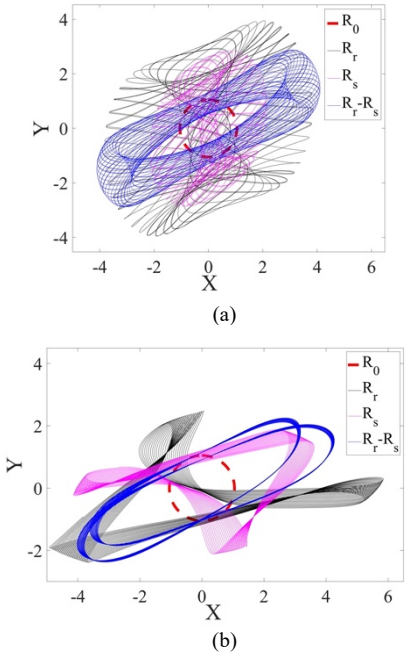

(a)

(b)

Fig. 4. Rotor/stator orbits for partial rub with system parameters as depicted in Eq. (7), where it is supposed that the friction coefficient $\mu = 0.4$ and the coefficient of fluid hydrodynamic force $M_{ff} = 0.2$.

4.2 Global response of general fluid-rotor-stator rubbing system

Firstly, by setting the coefficient of the fluid hydrodynamic force to the extreme values, the critical rotating speed of no-rub motion can be discussed analytically according to the comparison between the relative deflection $|R_r - R_s|$ and the clearance R_0. As known, rubbing occurs when $|R_r - R_s| \geq R_0$. Therefore, the critical condition of the rotor/stator rubbing is $|R_r - R_s| = R_0$, which means pure rolling without friction in the no-rub motion. Based on Eq. (6), the governing equations of no-rub motion in the general fluid-rotor-stator rubbing system are obtained by the dynamic equilibrium without friction.

$$\begin{cases} (1-M_{ff})X_r'' + 2\zeta_r X_r' + X_r = \Omega^2 \cos\Omega\tau \\ (1+M_{ff})Y_r'' + 2\zeta_r Y_r' + Y_r = \Omega^2 \sin\Omega\tau \\ M_{sr}X_s'' + 2\zeta_s\sqrt{M_{sr}\beta_{sr}}X_s' + \beta_{sr}X_s = 0 \\ M_{sr}Y_s'' + 2\zeta_s\sqrt{M_{sr}\beta_{sr}}Y_s' + \beta_{sr}Y_s = 0 \end{cases} \tag{8}$$

(1) $M_{ff} = 0$

To delve into the fluence of the fluid hydrodynamic force on the critical rotating speed of no-rub motion, we first study the critical condition of the rotor/stator rubbing system with dry friction. By omitting the items related to friction, the governing equations with $M_{ff} = 0$ can be written as:

$$\begin{cases} X_r'' + 2\zeta_r X_r' + X_r = \Omega^2 \cos\Omega\tau \\ Y_r'' + 2\zeta_r Y_r' + Y_r = \Omega^2 \sin\Omega\tau \end{cases} \tag{9}$$

According to the positive frequency component corresponding to the rotating speed Ω in no-rub motion, the parameterization method can be used for the periodic solutions [14].

$$\begin{cases} X_r = R_{ru}\cos(\Omega\tau + \varphi) \\ Y_r = R_{ru}\sin(\Omega\tau + \varphi) \end{cases} \tag{10}$$

where $R_{ru} = \Omega^2 \Big/ \sqrt{(1-\Omega^2)^2 + (2\zeta_r\Omega)^2}$, $\tan\varphi = -2\zeta_r\Omega/(1-\Omega^2)$

Undoubtedly, the solutions from Eq. (10) are stable and available only when the amplitude of the rotor R_{ru} is less the clearance R_0 between the rotor and the stator, i.e., $R_{ru} < R_0$. Based on the critical condition $R_{ru} = R_0$ of the synchronous full annular no-rub motion, the parameterization function of the critical rotating speed Ω_0 of no-rub motion is constructed as:

$$(R_0^{\,2} - 1)\Omega_0^{\,4} + 2R_0^{\,2}(2\zeta_r^{\,2} - 1)\Omega_0^{\,2} + R_0^{\,2} = 0 \tag{11}$$

The critical rotating speed Ω_0 of no-rub motion can be simultaneously determined by solving Eq. (11). However, not all the solutions of Eq. (11) are meaningful to meet the

condition of the postulated solutions except for the positive solution pairs for the synchronous full annular no-rub motion. For the system parameters given by Eq. (7), four solutions of Ω_0 can be obtained in the calculation from Eq. (11). According to the feature of the solutions from X_r and Y_r, two meaningful solutions, Ω_{L0} and Ω_{U0}, among the four roots of Eq. (11) are in the calculation.

$$\begin{cases} \Omega_{L0} = 0.7160 \\ \Omega_{U0} = 4.5807 \end{cases} \tag{12}$$

Therefore, the synchronous full annular no-rub motion exists in the range of the rotating speed, which is smaller than Ω_{L0} or greater than Ω_{U0}.

(2) $M_{ff} = 1$

In a similar vein, by omitting the items related to friction, we can write the governing equations with $M_{ff} = 1$ as:

$$\begin{cases} 2\zeta_r X_r' + X_r = \Omega^2 \cos\Omega\tau \\ 2Y_r'' + 2\zeta_r Y_r' + Y_r = \Omega^2 \sin\Omega\tau \end{cases} \tag{13}$$

From $2\zeta_r X_r' + X_r = \Omega^2 \cos\Omega\tau$, it yields,

$$X_r = 2\Omega^2 \cos\Omega\tau - 4\zeta_r \tag{14}$$

As known, the critical condition for rubbing is $X_r^2 + Y_r^2 = R_0^2$. Then,

$$Y_r = \sqrt{R_0^2 - X_r^2} = \sqrt{R_0^2 - (2\Omega^2 \cos\Omega\tau - 4\zeta_r)^2} \tag{15}$$

Substituting Y_r, Y_r', and Y_r'' into Eq. (12), we can obtain the critical rotating speed Ω_{L0} of no-rub motion in the general fluid-rotor-stator rubbing system with $M_{ff} = 1$.

In the general fluid-rotor-stator rubbing system with the parameters given by Eq. (7), the analytical solutions of Eqs. (12) and (15) can be incorporated in the simulation results derived by the governing functions of Eq. (6) under the condition of $M_{ff} \in [0,1]$. Considering the friction effect between the stator the rotor in the fluid, the critical rotating speeds of no-rub motion can be depicted on the parameter plane of $\Omega - \mu$ with the variation of M_{ff}, as shown in Fig. 5. The curve Ω_{L0} of the critical rotating speed indicates the rotating speed, where the deflection of the linear rotor covers the clearance. Thus, the synchronous no-rub motion is in the rotating speed range less than Ω_{L0}. As shown in Fig. 5, the critical rotating speed decreases from 0.716 to 0.589 with the increase of the coefficient of the hydrodynamic force M_{ff} in the interval of $[0,1]$, which is subject to the hydrodynamic forces induced by the interaction between the rotor and the fluid. That is, when a disturbance of the hydrodynamic forces applied on the rotor is large enough to make the rotor rotating speed exceed the critical initial speed, the rotor/stator rubbing can be initiated with $|R_r - R_s| >> R_0$. Besides, the more powerful the hydrodynamic forces, the more likely it can trigger rubbing from synchronous no-rub motion.

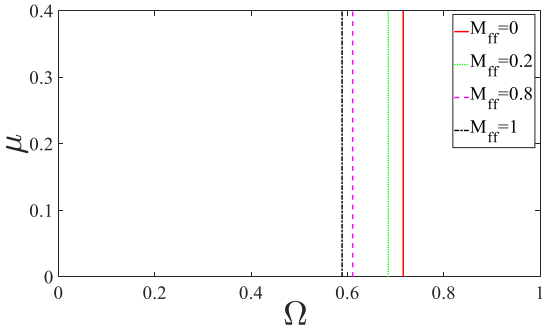

Fig. 5. Boundaries of no-rub motion on parameter plane $\Omega - \mu$ with the variation of M_{ff} and other system parameters as depicted in Eq. (7)

The examples with the system parameters as depicted in Eq. (7) are presented to illustrate the overall picture of the global response characteristics of the general fluid-rotor-stator rubbing system. As known from the preceding analytical solutions, the existence boundaries of no-rub motion are determined rigorously with high accuracy, which have also been proven by numerical simulations. Thus, the global response characteristics of the general fluid-rotor-stator rubbing system can be effectively demonstrated in the following analysis. Based on the simulation results from Eq. (6), the global response characteristics on the parameter plane of $\Omega - \mu$ with $M_{ff} = 0.2$ and $\mu = 0.4$ are depicted in Fig. 6.

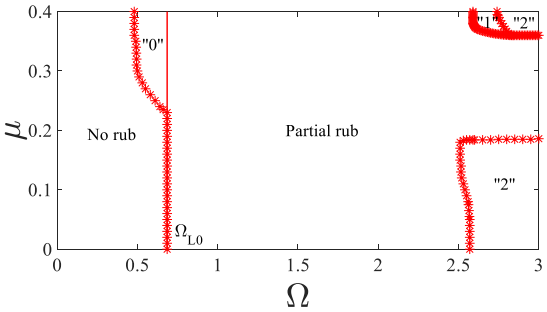

Fig. 6. Rotor response characteristics on parameter plane $\Omega - \mu$ with system parameters as depicted in Eq. (7). The regions of the three types of coexistence are identified. Ω_{L0} is the critical rotating speed of no-rub motion.

In the global response characteristics of Fig. 6, the curve Ω_{L0} representing the critical rotating speed of no-rub motion is 0.685. Then, the partial rub and heavy rub motion can be triggered and stopped as the variation of the rotor rotating speed Ω and the friction coefficient μ. On the parameter plane of $\Omega - \mu$, the parameter regions marked by numbers represent different regions of coexistence, i.e., 0 (no-rub motion + partial rub), 1 (partial rub + heavy rub), and 2 (heavy rub). It is straightforward to show that the partial rub exists already from a very low rotating speed when the friction coefficient is larger than a certain value as $\mu > 0.23$. This phenomenon satisfies the basic characteristics of the rotor/stator rubbing system with dry friction [5,15,33], which implicitly indicates that the energy of the rubbing responses dominantly comes from the friction rather than the hydrodynamic forces. Due to the coexistence of the partial rub and heavy rub (see region 1), the jump phenomenon can occur in this region. When the friction coefficient is under this value, i.e., $\mu \le 0.36$, one can find the regions of the partial rub. It is even worse a region exists (see region 2) where the heavy rub is the sole stable response for the

general fluid-rotor-stator rubbing system with $\mu \le 0.186$ and $\mu \ge 2.51$. So, it is quite possible to induce the more destructive heavy rub from a relatively mild rubbing response or even from partial rub when the rotor is subjected to a sudden outside disturbance. Besides, avoiding a higher rotating speed of the rotor and/or the large contact friction is important, especially that which exceeds the one defined by the criterion of the heavy rub. However, because of the hydrodynamic forces in the general fluid-rotor-stator rubbing system, the dry friction backward whirl shown in the rotor/stator rubbing system with dry friction [15] is not detected. Thus, from this point, we conclude that hydrodynamic forces in fluid are beneficial to mitigate the rotor/stator rubbing responses. Due to the influence of non-symmetrical hydrodynamic forces in the general fluid-rotor-stator rubbing system, the partial rub occupies most regions of the parameter plane $\Omega - \mu$, resulting from the asymmetric size of the major radius and minor radius of the elliptical orbit in the X and Y directions.

4.3 Influences of system parameters on relative deflection

From the discussion of the examples in subsection 4.2, we find that the rubbing responses in the general fluid-rotor-stator rubbing system are categorized into three types from the point of view of the relative deflection between the rotor and the stator, and their appearance depends on the system parameters. To gain a systematic overview of how the system parameters affect the relative deflection, the major relative deflection $|R_r - R_s|_{\max}$ and the minor relative deflection $|R_r - R_s|_{\min}$ versus the rotating speed are shown on the parameter planes of $|R_r - R_s|_{\max}$ - Ω and $|R_r - R_s|_{\min}$ - Ω, with different mass ratio M_{sr}, stiffness ratio β_{sr}, and rotor radius R_d at the contact point.

4.3.1 Influence of mass ratio M_{sr} on relative deflection

By fixing $\zeta_r = 0.02$, $\zeta_s = 0.01$, $\beta_{cr} = 20$, $\beta_{sr} = 15.319$, $R_0 = 1.05$, $R_d = 2.66R_0$, $M_{ff} = 0.2$, the plots of $|R_r - R_s|_{\max}$ - Ω and $|R_r - R_s|_{\min}$ - Ω with $\Omega \in [0.69, 1.2]$ and different mass ratio M_{sr} are respectively shown in Fig. 7.

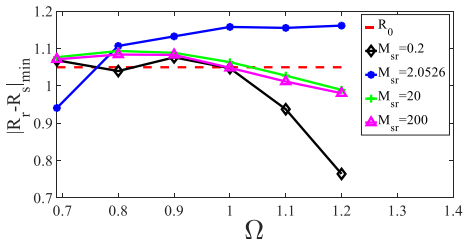

(a) Minor relative deflection $|R_r - R_s|_{\min}$ - Ω

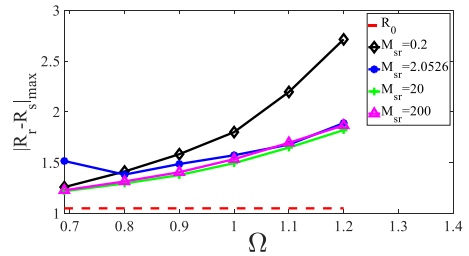

(b) Major relative deflection $|R_r - R_s|_{\max}$ - Ω

Fig. 7. Plots of minor and major relative deflections with different rotor mass M_{sr} when $\zeta_r = 0.02$, $\zeta_s = 0.01$, $\beta_{cr} = 20$, $\beta_{sr} = 15.319$, $R_0 = 1.05$, $R_d = 2.66R_0$, $M_{ff} = 0.2$, and $\mu = 0.4$

As shown in Fig. 7(a), when the contact surfaces have a special mass ratio, i.e., $M_{sr} = 2.0526$, the minor relative deflection $|R_r - R_s|_{\min}$ gradually grows larger and ends up around 1.16 with the increase of the rotating speed Ω. Interestingly, for $M_{sr} = 0.2$, $M_{sr} = 20$, or $M_{sr} = 200$, the minor relative deflection $|R_r - R_s|_{\min}$ possesses a maximum point nearly $\Omega \approx 0.9$. Thus, it does not always monotonically increase as in the case of a great mass ratio, i.e., $M_{sr} \ge 20$, with the increase of the rotating speed. In addition, for $\Omega \in [0.69, 1.2]$, the minor relative deflection is partly greater than the clearance between the rotor and the stator, i.e., $|R_r - R_s|_{\min} \ge R_0$ or $|R_r - R_s|_{\min} < R_0$. As shown in Fig. 7(b), the major relative deflection $|R_r - R_s|_{\max}$ is always greater than the clearance R_0 and becomes greater with the increase of the rotating speed Ω. As $|R_r - R_s|_{\min} > R_0$, the rubbing responses are determined by the minor relative deflection $|R_r - R_s|_{\min}$ just as it changes across R_0 from the small to the large one, namely, switching from $|R_r - R_s|_{\min} < R_0$ to $|R_r - R_s|_{\min} \ge R_0$. Also, as shown in Fig. 7(b), the major relative deflections of $M_{sr} = 0.2$, $M_{sr} = 20$, and $M_{sr} = 200$ are almost coincident when $\Omega \ge 1.1$. Thus, we conclude that the major relative deflection $|R_r - R_s|_{\max}$ becomes continuously smaller as the mass ratio M_{sr} increases. When the mass ratio M_{sr} increases to at least 20, the relative deflection between the rotor and the stator fluctuates within a narrow range. It is straightforward to show that the switching scenario between the partial rub and heavy rub occurs with the variation of mass ratio M_{sr}.

4.3.2 Influence of stiffness ratio β_{sr} on relative deflection

Fixing $\zeta_r = 0.02$, $\zeta_s = 0.01$, $\beta_{cr} = 20$, $M_{sr} = 2.0526$, $R_0 = 1.05$, $R_d = 2.66R_0$, $M_{ff} = 0.2$ shows the plots of $|R_r - R_s|_{\max}$ - Ω and $|R_r - R_s|_{\min}$ - Ω with $\Omega \in [0.69, 1.2]$ and different stiffness ratio β_{sr} in Fig. 8.

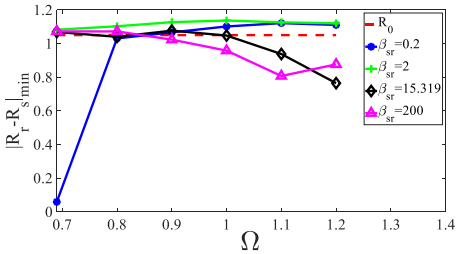

(a) Minor relative deflection $|R_r - R_s|_{\min}$ - Ω

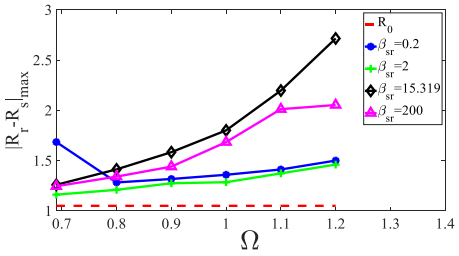

(b) Major relative deflection $|R_r - R_s|_{\max}$ - Ω

Fig. 8. Plots of minor and major relative deflections with various stiffness ratio β_{sr} when $\zeta_r = 0.02$, $\zeta_s = 0.01$, $\beta_{cr} = 20$, $M_{sr} = 2.0526$, $R_0 = 1.05$, $R_d = 2.66R_0$, $M_{ff} = 0.2$, and $\mu = 0.4$

Interestingly, Fig. 8(a) shows that when the contact surfaces have small stiffness ratio, i.e., $\beta_{sr} = 0.2$ and $\beta_{sr} = 2$, the minor relative deflection $|R_r - R_s|_{\min}$ gradually grows larger and ends up around 1.2 with the increase of the rotating speed Ω. When $\beta_{sr} \geq 15.319$, the minor relative deflection $|R_r - R_s|_{\min}$ becomes increasingly smaller with the increase of Ω. In addition, for $\Omega \in [0.69, 1.2]$, the minor relative deflection is partly greater than the clearance between the rotor and the stator, i.e., $|R_r - R_s|_{\min} \geq R_0$ or $|R_r - R_s|_{\min} < R_0$. As shown in Fig. 8(b), the major relative deflection $|R_r - R_s|_{\max}$ is always greater than the clearance R_0 and becomes even greater with the increase of the rotating speed Ω. When $\beta_{sr} = 15.319$, the major relative deflection is greater than that with the stiffness ratio larger or smaller than 15.319. Fig. 8(b) also shows that the major relative deflections of $\beta_{sr} = 0.2$ and $\beta_{sr} = 2$ are almost coincident when $\Omega \geq 1.1$. In combination, the relative deflection between the rotor and the stator fluctuates within a narrow range. The switching scenario between the partial rub and heavy rub also occurs with the variation of stiffness ratio β_{sr}. Comparison with the results in Fig. 7 shows that the increase of mass ratio M_{sr} has an effect equivalent to a decrease in stiffness ratio β_{sr}, which causes the relative deflection between the rotor and stator to become smaller. This condition can also emerge in the rotor/stator rubbing system with dry friction [33].

4.3.3 Influence of rotor radius R_d on relative deflection

Fixing $\zeta_r = 0.02$, $\zeta_s = 0.01$, $\beta_{cr} = 20$, $\beta_{sr} = 15.319$, $R_0 = 1.05$, $M_{sr} = 2.0526$, $M_{ff} = 0.2$, shows the plots of $|R_r - R_s|_{\max}$ - Ω and $|R_r - R_s|_{\min}$ - Ω with $\Omega \in [0.69, 1.2]$ and different rotor radius R_d in Fig. 9.

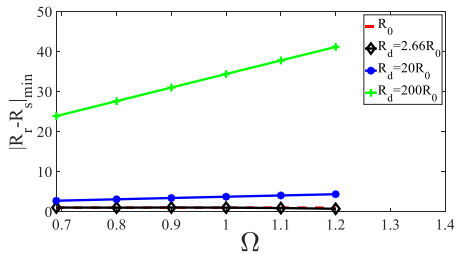

(a) Minor relative deflection $|R_r - R_s|_{\min}$ - Ω

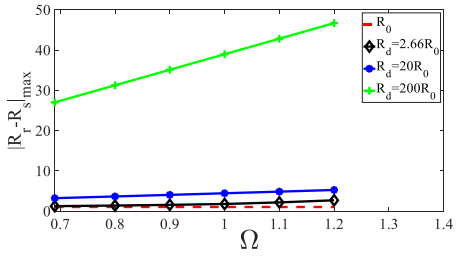

(b) Major relative deflection $|R_r - R_s|_{\max}$ - Ω

Fig. 9. Plots of minor and major relative deflections with different rotor radius R_d when $\zeta_r = 0.02$, $\zeta_s = 0.01$, $\beta_{cr} = 20$, $\beta_{sr} = 15.319$, $R_0 = 1.05$, $M_{sr} = 2.0526$, $M_{ff} = 0.2$, and $\mu = 0.4$

Interestingly, according to Fig. 9(a), when the contact surfaces own small rotor radius, i.e., $R_d = 2.66R_0$, the minor relative deflection fluctuates around the clearance, namely, $|R_r - R_s|_{\min} \approx R_0$, as the increase of the rotating speed Ω. Then, the minor relative deflection $|R_r - R_s|_{\min}$ becomes increasingly greater with the increase of rotor radius R_d. Besides, when $R_d \geq 20R_0$, the minor relative deflection $|R_r - R_s|_{\max}$ is always greater than the clearance R_0, i.e., $|R_r - R_s|_{\max} > R_0$. As shown in Fig. 9(b), the major relative deflection $|R_r - R_s|_{\max}$ is always greater than the clearance R_0 and becomes even greater as the rotating speed Ω increases. In addition, the major relative deflection $|R_r - R_s|_{\max}$ gradually grows bigger with the increase of rotor radius R_d. Obviously, as the rotor radius R_d increases, the relative deflection between the rotor and stator becomes greater and can induce the switching scenario between the partial rub and heavy rub in the general fluid-rotor-stator rubbing system.

To conclude, (1) the switching scenario between the partial rub and heavy rub can be introduced by the variation of the system parameters in the general fluid-rotor-stator rubbing system. (2) Due to the reverse influences of mass ratio M_{sr} and stiffness ratio β_{sr} on the relative deflection, the rubbing responses can be mitigated by the decrease of the rotor mass m_r and/or the increase of the rotor stiffness in a certain range of M_{sr} and β_{sr}, for example, $M_{sr} < 20$ or $\beta_{sr} > 2$ in the above case. (3) The heavy rub can be initiated by the increase of rotor radius R_d and/or decrease of the clearance R_0 between the rotor and stator in the general fluid-rotor-stator rubbing system. (4) The major relative deflection $|R_r - R_s|_{\max}$ and minor relative deflection $|R_r - R_s|_{\min}$ exhibit variations as the rotating speed Ω of the rotor increases.

5. Conclusions

To explore the global response characteristics of the general fluid-rotor-stator rubbing system widely applied in rotating machinery, we established a 4D fluid-rotor-stator rubbing system considering the dynamics of the rotor and stator, the dry friction and flexibility on the contact surfaces, as well as the fluid-rotor interaction. Through theoretical analysis and numerical simulations, three types of rubbing responses and their critical conditions were conducted as the variation of the system parameters and initial conditions. The following conclusions can be drawn:

(1) According to the orbits and full spectra, the rotor in the general fluid-rotor-stator rubbing system successively undertakes the no-rub motion, partial rub, and heavy rub as the rotating speed increases.

(2) As the critical rotating speed of the no-rub motion decreases from 0.716 to 0.589 with the increase of the coefficient of the hydrodynamic force M_{ff} in the interval of $[0,1]$, the hydrodynamic forces can cause rubbing to occur easily in the general fluid-rotor-stator rubbing system.

(3) The coexistence of the partial rub with other responses can be observed, and the partial rub can be induced to occupy most regions of the parameter plane of friction coefficient and rotating speed. Compared to the rubbing responses in the rotor/stator rubbing system with dry friction, the rubbing responses in the general fluid-rotor-stator rubbing system can be mitigated by the hydrodynamic forces in fluid.

(4) Studying the influences of the system parameters on the relative deflection in the general fluid-rotor-stator rubbing system shows the interplay among the system parameters. For instance, under the condition of $M_{sr} \le 20$ and $\beta_{sr} \ge 2$, the decrease of the rotor mass at a given stiffness ratio has the same effect of increasing the rotor stiffness at a given mass ratio for the control of the rubbing responses. On the other hand, the increase of the rotor radius at the contact for a given clearance has the same effect of decreasing the clearance at a given rotor radius to increase the amplitudes of the rubbing responses.

Thus, the 4D fluid-rotor-stator rubbing system is deeply studied for the global response characteristics by theoretical analysis and numerical simulations. However, the hydrodynamic forces can also exert an additional effect on the rubbing responses of the rotor/stator system, such as the fluid-stator interaction, which should be explored in future studies.

Acknowledgements

This work was supported by Interdisciplinary Research Project of Nanyang Institute of Technology (Grant No. 520065), Key Scientific Research Projects of Colleges and Universities in Henan Province (Grant No. 22B470009) and Key R&D Projects in Sichuan Province (Grant No. 2022YFG0060).

References

1. Ma Y., Martinez V. P., Baniotopoulos C., "Wind turbine tower collapse cases: a historical overview". *Proceedings of the Institution of Civil Engineers-Structures and Buildings*, 172(8), 2019, pp. 547-555.
2. Prabith K., Krishna I. R. P., "The numerical modeling of rotor-stator rubbing in rotating machinery: a comprehensive review". *Nonlinear Dynamics*, 101(2), 2020, pp.1317-1363.
3. Aneesh G. N., Sandeep S. U., Sanjay K. S., "Role of artificial intelligence in rotor fault diagnosis: a comprehensive review". *Artificial Intelligence Review*, 54, 2021, pp.2609-2668.
4. Gabriele P., Riccardo T., Silvia C. S., Sergio M. S., Gerhard D., "Feature extraction from multi-axis MEMS sensors for unbalance detection in non-stationary rotating conditions". *Mechatronics*, 83, 2022, pp.102762.
5. Muszynska A., "*Rotordynamics*". New York: Taylor & Francis, USA, 2005, pp.58-296.
6. Ishida Y., Yamamoto T., "*Linear and nonlinear rotordynamics*". Weinheim: Wiley-VCH, Germany, 2012, pp.120-177.
7. Sváček P., "Numerical solution of fluid-structure interaction problems with considering of contacts". *Acta Polytechnica*, 61(SI), 2021, pp.155-162.
8. Bazilevs Y., Takizawa K., Tezduyar T. E., "*Computational fluid-structure interaction: methods and applications*". Hoboken: John Wiley & Sons, USA, 2013, pp.11-196.
9. Dimarogonas A. D., Sandor G. N., "Packing rub effect in rotating machinery, part I: a state of the art review". *Wear*, 14(3), 1969, pp.153-170.
10. Jacquet-Richardet G., Torkhani M., Cartraud P., Thouverez F., Nouri Baranger T., Herran M., Gibert C., Baguet S., Almeida P., Peletanab L., "Rotor to stator contacts in turbomachines: review and application". *Mechanical Systems and Signal Processing*, 40(2), 2013, pp.401-420.
11. Aqiang L., Gaowen L., Xinxin W., Qing F., "Comprehensive evaluations on performance and energy consumption of pre-swirl rotor-stator system in gas turbine engines". *Energy Conversion and Management*, 244, 2021, pp.114440.
12. Shunzeng W., Ling H., Jun J., "Nonsmooth behavior of sliding bifurcations in a general piecewise smooth rotor/stator rubbing system". *International Journal of Bifurcation and Chaos*, 31(2), 2021, pp.2150085.
13. Zigang L., Jun J., Jing L., Ling H., Ming L., "A subdomain synthesis method for global analysis of nonlinear dynamical systems based on cell mapping". *Nonlinear Dynamic*, 95, 2019, pp.715-726.
14. Shunzeng W., Ling H., Jun J., "Evaluation on spectral submanifold based reduced models of a rotor/stator rubbing system with cross-coupling stiffness". *International Journal of Mechanical Sciences*, 228, 2022, pp.107486.
15. Jiang J., Ulbrich H., "Stability analysis of sliding whirl in a nonlinear Jeffcott rotor with cross-coupling stiffness coefficients". *Nonlinear Dynamics*, 24(3), 2001, pp.269-283.
16. Vlajic N., Champneys A. R., Balachandran B., "Nonlinear dynamics of a Jeffcott rotor with torsional deformations and rotor-stator contact". *International Journal of Non-Linear Mechanics*, 92, 2017, pp.102-110.
17. Varney P., Green I., "Rough surface contact of curved conformal surfaces: an application to rotor-stator rub". *Journal of Tribology*, 138(4), 2016, pp.041401.
18. Elijah C., Shaw A. D., Friswell M. I., "Frictional effects on the nonlinear dynamics of an overhung rotor". *Communications in Nonlinear Science and Numerical Simulation*, 78, 2019, pp.104875.
19. Nikiforov A., "Whip velocity of backward whirl with slip in multiple-degree-of-freedom rotor-stator system". *Mathematical Models in Engineering*, 5(4), 2019, pp.146-157.
20. Alfredo G., Alfred F., Mònica E., Carme V., Eduard E., "Characterization of the effects of ingested bodies on the rotor-stator interaction of hydraulic turbines". *Energies*, 14(20), 2021, pp.6669.
21. Bernard X. T. K., Alfayo A. A., "Fluid forces as an additional source of vibration in a rotor-stator rub system". In: *2021 IEEE 12th International Conference on Mechanical and Intelligent Manufacturing Technologies*, Cape Town, South Africa: IEEE, 2021, pp.115-121.
22. Bernard X. T. K., Alfayo A. A., "Experimental study of the impact of the fluid forces on disturbances induced by the rotor-stator rubbing". In: *2021 IEEE 12th International Conference on Mechanical and Intelligent Manufacturing Technologies*, Cape Town, South Africa: IEEE, 2021, pp.133-138.
23. Kadyrov S. G., Wauer J., Sorokin S. V., "A potential technique in the theory of interaction between a structure and a viscous, compressible fluid". *Archive of Applied Mechanics*, 71(6-7), 2016, pp.405-417.
24. Kydyrbekuly A., Khajiyeva L., Gulama-Garyp A. Y., Kaplunov J., "Nonlinear vibrations of a rotor-fluid-foundation system supported by rolling bearings". *Journal of Mechanical Engineering*, 62(6), 2016, pp.351-362.

25. Bernard X. T., Desejo F. S., Alfayo A., "Influences of hydrodynamic forces on the identification of the rotor-stator-rubbing fault in a rotating machinery". *International Journal of Rotating Machinery*, 2020(6), 2020, pp.8816191.
26. Gomes J. P., Lienhart H., "Fluid-structure interaction-induced oscillation of flexible structures in laminar and turbulent flows". *Journal of Fluid Mechanics*, 715, 2013, pp.537-572.
27. Xiang L., Hu A., Hou L., Xiong Y., Xing J., "Nonlinear coupled dynamics of an asymmetric double-disc rotor-bearing system under rub-impact and oil-film forces". *Applied Mathematical Modelling*, 40(7-8), 2016, pp.4505-4523.
28. Banakh L., Nikiforov L., "Vibroimpact regimes and stability of system "rotor-sealing ring". *Journal of Sound and Vibration*, 308(3-5), 2007, pp.785-793.
29. Rui Z., Guangchao W., Qingpeng H., Anlei Z., Jianxing R., Xin X., "Dynamic characteristics and experimental research of a two-span rotor-bearing system with rub-impact fault". *Shock and Vibration*, 2019(1), 2019, pp.6309809.
30. Hengstler J. A. N., "*Influence of the fluid-structure interaction on the vibrations of structures*". Doctoral dissertation of ETH Zurich, Switzerland, 2013, pp.2-110.
31. Presas A., Egusquiza E., Valero C., Valentin D., Seidel U., "Feasibility of using PZT actuators to study the dynamic behavior of a rotating disk due to rotor-stator interaction". *Sensors*, 14(7), 2014, pp.11919-11942.
32. Lahriri S., Weber H. I., Santos I. F., Hartmann H., "Rotor-stator contact dynamics using a non-ideal drive-theoretical and experimental aspects". *Journal of Sound and Vibration*, 331(20), 2012, pp.4518-4536.
33. Shunzeng W., Ling H., Jun J., "Characteristics of stick-slip oscillations in dry friction backward whirl of piecewise smooth rotor/stator rubbing systems". *Mechanical Systems and Signal Processing*, 135, 2020, pp.106387.